AIMS Materials Science, 10(1): 112–138.
DOI: 10.3934/matersci.2023007
Received: 31 July 2022
Revised: 07 December 2022
Accepted: 13 December 2022
Published: 17 January 2023

http://www.aimspress.com/journal/Materials

Research article

Investigation of novel turbulator with and without twisted configuration under turbulent forced convection of a CuO/water nanofluid flow inside a parabolic trough solar collector

Omar Ouabouch[1,*], Imad Ait Laasri[2,3], Mounir Kriraa[4] and Mohamed Lamsaadi[1]

[1] Research Laboratory in Physics and Sciences for Engineers (LRPSI), Polydisciplinary Faculty, Sultan Moulay Slimane University, B. P 592, Beni-Mellal, Morocco
[2] Laboratory (LaMEE), Faculty of Sciences Semlalia, Cadi Ayyad University, Marrakesh, Morocco
[3] Green Energy Park (IRESEN, UM6P), Benguerir, Morocco
[4] Laboratory of Engineering, Industrial Management and Innovation, Faculty of Sciences and Technologies, Hassan 1st University, Settat, Morocco

* **Correspondence:** Email: ouabouch.omar@gmail.com.

Abstract: In this study, we numerically investigated the hydrothermal performance of a parabolic trough solar collector system in which nanofluids are used to transfer thermal energy. The single-phase model has been used to evaluate the respective influences of the spherical shape of nanoparticles with a volume fraction of (φ = 3%), Reynolds number varying between 50,000 ≤ Re ≤ 250,000 and the insertion of a turbulator with and without a twisted configuration on the hydrothermal characteristics created by the turbulent forced convection of a CuO/water nanofluid. The shaped turbulator (+) inserted in the absorber tube had a length turb_L = 2.4 m, a height turb_H = 40 mm and a width turb_t = 2 mm. In the second configuration, the considered turbulator was twisted (N_twist = 5, 10 and 15 twists). The turbulator was positioned at 0.6 m from the inlet of the tube and 1 m from the outlet of the collector. The studied performances included the heat transfer characteristics, pressure drop, friction factor, thermal efficiency, temperature and velocity distribution of the outlet field. The most significant contribution of this study is the proposal of the best parameters to increase the thermal and hydraulic efficiency of parabolic troughs by adding a new turbulator with the considered twists.

Keywords: parabolic trough solar collector; nanofluid; turbulator; turbulator twisted; hydrothermal characteristics

1. Introduction

Today, the global situation of air and water pollution, as well as climate change, demand the replacement of fossil fuels with other energy sources, such as solar energy [1]. Parabolic trough solar collectors are the most successful, widely used and advanced alternative to fossil fuel power plants, and they provide heat at medium and high temperatures for a variety of applications. In view of the large application of this type of collector, a number of methods have been proposed to improve their performance, as related both to their structure and the type of working fluid [2]. Studies have been conducted on the improvement of parabolic trough solar collectors in order to increase their efficiency at high degrees of operating temperature. A numerical study was carried out by Ouabouch et al. [3] on the effects of flow regime and geometrical parameters on the performance of a parabolic trough solar collector based on a nanofluid (CuO/water). They concluded that the length of the collector, the internal diameter of the absorber and the concentration factor, as well as the type of nanofluid and its volume concentration, have considerable effects on its performance. Tembhare et al. [4] examined the performance of nanofluids in solar thermal and photovoltaic systems. They have detailed the properties of nanofluids for solar thermal applications (experimental and numerical investigations) with conventional experimental setups. The effects of nanoparticle concentration, flow rate, ambient temperature, solar intensity and inlet temperature on the performance of the solar thermal system is also discussed. Qi et al. [5] applied a TiO_2/water nanofluid at different concentrations in a double-tube heat exchanger. Their findings indicated that the use of the nanofluid might result in a 14.8% improvement in heat transfer compared to the use of pure water. Recently, nanofluid science has been considered as an effective technique for improving cooling/heating systems in many industrial applications. Nanofluids are fluids containing nanoparticles of size 1 to 100 nm that are suspended in base fluids such as ethylene glycol water [6]. Ouabouch et al. [7] discussed the methods of the fabrication of nanofluids, their thermophysical properties and their application in solar collectors, with focus on their ability to improve the efficiency of these collectors. A study on the use of Al_2O_3 and CuO nanoparticles in water for parabolic trough solar collectors was conducted by Ghasemi and Ranjbar [8]. The researchers found an improvement in the heat transfer coefficient of about 28% with Al_2O_3 and 35% with CuO. Ouabouch et al. [9] performed a comparative study of four different nanofluids, i.e., CuO (3%), Al_2O_3 (6%), SiO_2 (4.82%) and TiO_2 (3.15%), in a parabolic trough solar collector. The aim was to numerically examine the heat transfer and field flow characteristics of these nanoparticles with different concentrations to maintain the same price and evaluate them against each other. The authors concluded that the nanoparticles CuO and Al_2O_3 resulted in the best performance among all of the studied materials. Recently, the researchers also investigated the use of corrugated tubes and the insertion of turbulators in the absorber as methods of thermal enhancement. Bellos et al. [10] employed a sinusoidal absorber tube in a parabolic trough solar collector, using nanofluids to evaluate its performance. It showed an increase in thermal efficiency of about 4.55%. Garcia et al. [11] employed a helical arrangement in a pipe to achieve a homogeneous fluid flow in the transition zone. They found a higher Nu in the system under study. Mwesigye et al. [12] performed a numerical study on the thermal and thermodynamic performance of a parabolic trough

collector solar receiver with perforated plate inserts. They concluded that a perforated plate insert enhanced the performance of the parabolic trough collector solar receiver tube. Khan et al. [13] studied and compared the results of nanofluid flow through heat-absorbing tubes of different geometries; they found a significant effect of geometry change on thermal efficiency. Liu et al. [14] analyzed the behavior of the double-twisted ribbon on the parabolic trough solar collector for use in direct steam generation systems. Their results indicate that the longitudinal vortices in the absorber tube significantly decreases the boundary temperature difference by about 39%. Saedodin et al. [15] studied the effect of twisted ribbons on the thermal performance of the parabolic trough solar collector. As a result, the maximum thermal transfer rate in the parabolic solar collector with twisted ribbon was 51.43%. In addition, a higher number of twisted ribbons and longitudinal ratio improved the thermal performance of the collector. The effects of phase change materials in a solar collector equipped with U-shaped helical tubes were studied. The results show that the use of toothed U-shaped helical tubes obtained a maximum thermal efficiency of 21.55% relative to simple helical tubes [16]. Fan et al. [17] employed a magnetic nanofluid (Fe_3O_4/water) with perforated twisted tape to improve the thermal performance of the heat exchanger. According to the exergy analysis, the thermo-hydraulic performance increases with increasing perforation rate up to a certain limit value, but it decreases beyond this limit value. The thermal performance of the heat transfer system is highly dependent on the magnetic field. The vertical magnetic field increases the heat transfer, while the parallel magnetic field decreases the system performance. Song et al. [18] investigated the effect of inserting a helical screw strip inside the absorber tube numerically. They found that the thermal losses can be decreased and the temperature can be maximized compared to the smooth tube, whereas the pressure drop increases by about five times relative to the straight case. The insertion of turbulators inside the absorber increases the turbulence and the heat exchange surface; in combination with the use of nanofluids, the aim is to improve the heat transfer by minimizing the pressure losses. In this study, the effects of different inlet Reynolds numbers $50{,}000 \leq Re \leq 250{,}000$, a CuO/water nanofluid with a volume fraction of 3%, various heights of the turbulator (turb_H = 30, 40 and 50 mm), different thicknesses (turb_t = 2, 4, 8 and 16 mm) and a turbulator with twists (N_twist = 5, 10 and 15 twists) were studied to evaluate the heat transfer and regime flow of the parabolic trough collector.

2. Physical configuration

2.1. Geometry and boundary conditions

The geometry of the parabolic trough solar collector is shown in Figure 1. The length of the absorber tube was L = 4 m, the inner diameter was 66 mm, with a thickness (t) of 2 mm. The length of the turbulator considered was 2.4 m. Similarly, the distance between the turbulator and the inlet was 0.6 m, and the outlet of the collector was 1 m. The receiver was assumed to be symmetrical about its vertical axis, so only half of the absorber tube of the receiver was considered for modeling. Boundary conditions of symmetry were applied for the receiver. Under the inlet condition, the fluid enters with a uniform velocity and a temperature of 300 K and the wall of the receiver tube was non-slip and without penetration. The outer wall was subjected to a non-uniform heat flux: for the upper half, $q' = I_{global}$ = 825 W/m^2, and for its lower part, $q' = I_{beam}.C_{ratio}$, with I_{beam} = 600 W/m^2 and C_{ratio} = 20. The pressure was set to equal the atmospheric pressure under the receiver output condition.

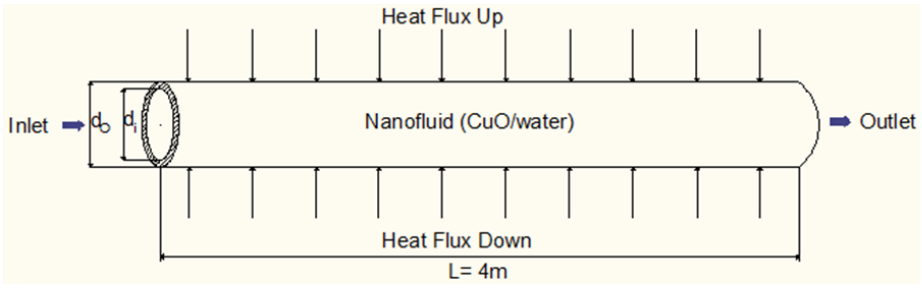

(a)

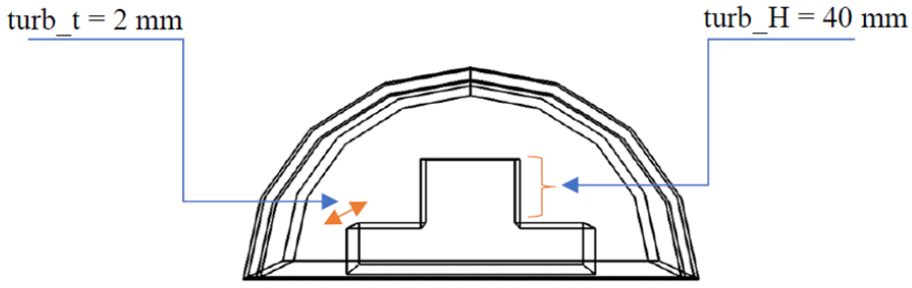

(b)

Figure 1. (a) Parabolic cylindrical collector schematic studied, (b) geometrical characteristics of the turbulator.

2.2. Thermophysical properties of the nanofluid

The main properties of the base fluid and nanoparticles are shown in Table 1. Furthermore, the thermophysical properties of the nanofluid with spherical-form nanoparticles with a diameter equal to 30 nm were determined by using the following equations:
Density [19]:

$$\rho_{nf} = (1-\varphi)\rho_f + \varphi\rho_s \tag{1}$$

Specific heat [20]:

$$(C_p)_{nf} = \frac{(1-\varphi)(\rho C_p)_f + \varphi(\rho C_p)_s}{\rho_{nf}} \tag{2}$$

Dynamic viscosity [21]:

$$\mu_{nf} = \frac{\mu_f}{(1-\varphi)^{2.5}} \tag{3}$$

Thermal conductivity [22]:

$$k_{nf} = \left(\frac{k_s+2k_f+2(k_s-k_f)\varphi}{k_s+2k_f-(k_s-k_f)\varphi}\right)k_f \tag{4}$$

Table 1. Thermophysical properties of material and base fluid [23].

Properties	Water	CuO
(kg/m^3)	998.9	6500
C_p(J/kg·K)	4188.3	540
K (W/m·K)	0.6352	18

2.3. Governing equations

A turbulent steady-state flow in a three-dimensional model was considered. The governing equations are the continuity equation, the Reynolds averaged Navier-Stokes equations and the averaged energy equations, which are given as follows [24]:
Continuity equation:

$$\nabla \cdot \left(\rho_{nf} V\right) = 0 \tag{5}$$

Momentum equation:

$$\nabla \cdot \left(\rho_{nf} VV\right) = -\nabla \cdot P + \nabla \cdot \left(\mu_{nf} \nabla V\right) \tag{6}$$

Energy equation:

$$\nabla \cdot \left(\rho_{nf} V C_{p,nf} T\right) = \nabla \cdot (K \nabla T) \tag{7}$$

2.4. Data analysis

The heat transfer coefficient is given by

$$h = \frac{q^{'}}{(T_{wi} - T_{ref})} \tag{8}$$

The Nusselt number is defined as

$$N_u = \frac{h \cdot d_i}{k_f} \tag{9}$$

The Reynolds number is calculated by

$$R_e = \frac{\rho_f \cdot U \cdot d_i}{\mu_f} \tag{10}$$

The Prandtl number is written as

$$P_r = \frac{\mu_f}{\rho_f . \alpha_f} \tag{11}$$

The friction factor is calculated by

$$f = \frac{2 \cdot \Delta P \cdot d_i}{L \cdot \rho \cdot U_{in}^2} \tag{12}$$

$$\Delta P = P_{av,inlet} - P_{av,outlet} \tag{13}$$

The thermal efficiency is calculated as follows:

$$\eta_{th} = \frac{Q_u}{Q_s} \tag{14}$$

$$Q_u = \dot{m}\, C_p\, (T_{out} - T_{in}) \tag{15}$$

$$Q_s = A_a \cdot I_{beam} \tag{16}$$

3. Numerical simulation

The present investigation examines the heat transfer and fluid flow inside a three-dimensional, steady-state receiving pipe, the RANS *k-ε* turbulence model has been used to model the turbulent flow with a single-phase approach [25]. A Computational Fluid Dynamics (CFD) simulation was performed to analyze the governing Eqs 5–7 to predict the velocity, pressure and temperature fields. The governing equations have been converted to algebraic equations by using the finite element method (FEM) scheme.

3.1. Grid independence

In the present study, the computational domain is an unstructured mesh of tetrahedral cells (Figure 2). An acceptable mesh was found by testing three grids (439700, 513477 and 878692 cells). The average Nusselt number and friction factor were approximated for the three grids, and the results were also compared. Based on the comparison of the results (Figures 3 and 4), the 513477-cell grid was considered as adequate for the current study.

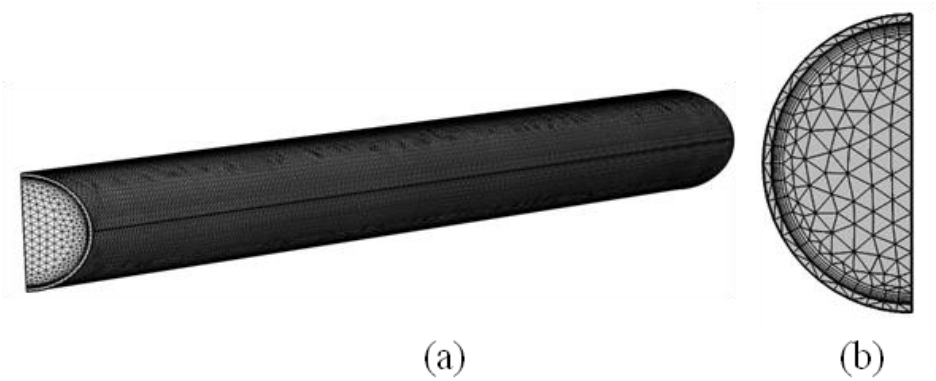

Figure 2. (a) Longitudinal view of the grid generated, (b) cross-sectional view.

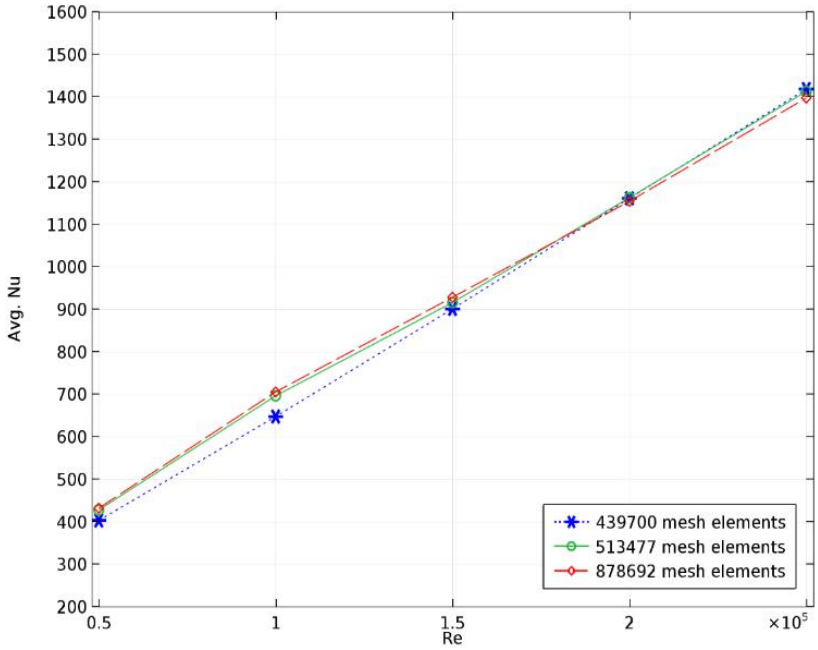

Figure 3. Grid independence studied for the average Nusselt number.

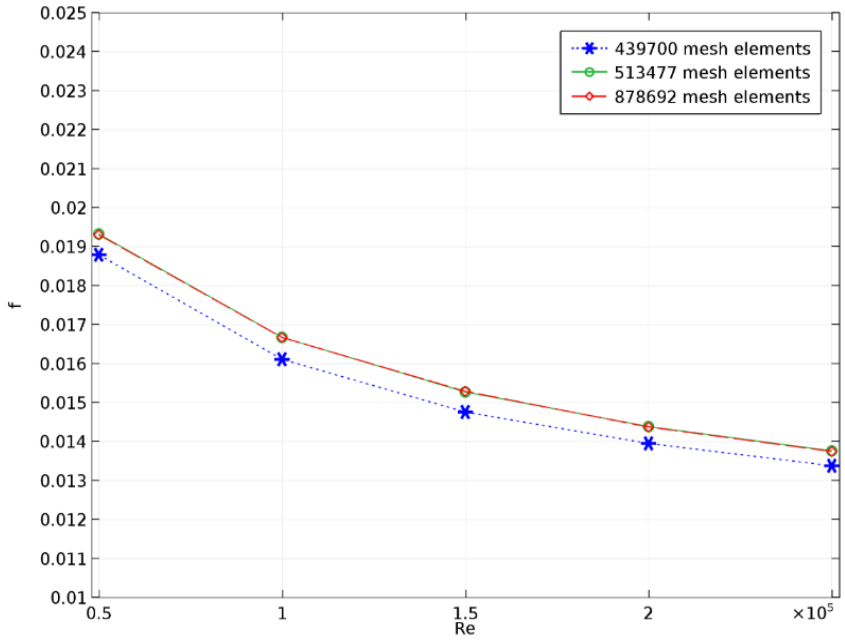

Figure 4. Grid independence studied for the friction factor.

3.2. Model validation

The results of the present research were compared with the results of Petukhov correlations [26] to prove the agreement of the results from the present numerical method. The values of the average Nusselt number and friction factor that were computed by the present CFD method were compared with those evaluated by using Eqs 17 and 18. Figures 5 and 6 present the results of the comparison.

As can be concluded, the maximum errors for Nu and f were 12% and 8%, respectively.

The Nusselt number is given as:

$$N_u = \frac{\left(\frac{f}{8}\right)(R_e P_r)}{1.07+12.7} \tag{17}$$

The friction factor is written as follows [26]:

$$f = (0.79 \cdot L_n \cdot R_e - 1.64)^{-2} \tag{18}$$

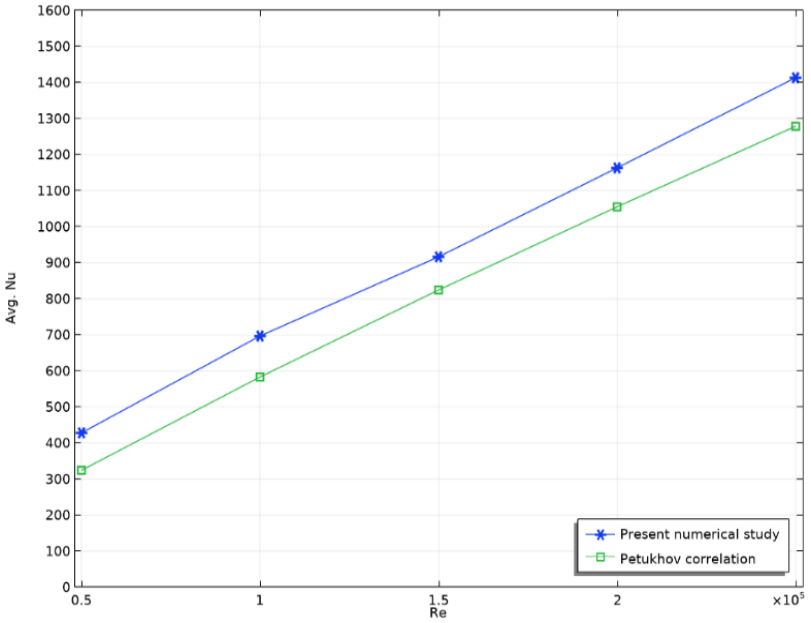

Figure 5. Validation of the average Nusselt number from the present work based on Petukhov correlations.

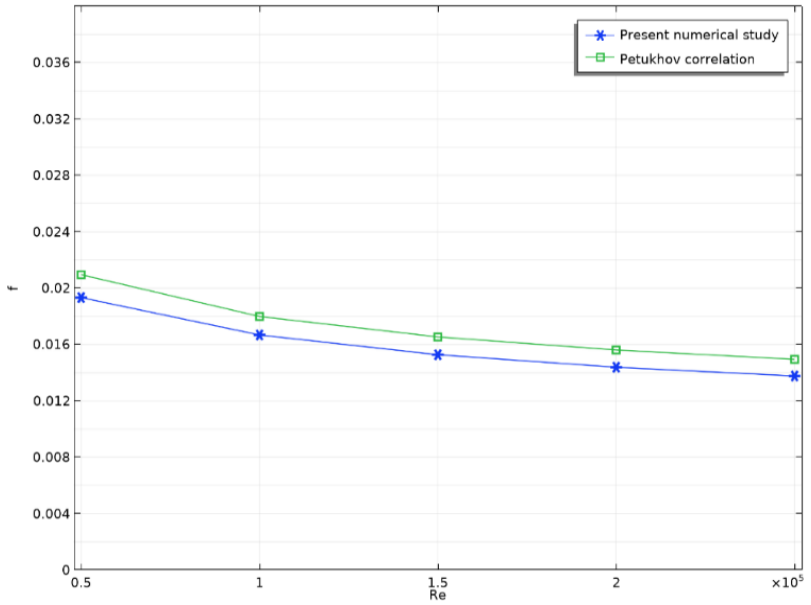

Figure 6. Validation of friction factor from the present work based on Petukhov correlations.

4. Results and discussions

4.1. Effect of turbulator geometry

4.1.1. Case 1: Turbulator thickness (turb_t) = 2 mm, with different turbulator heights (turb_H = 30, 40 and 50 mm)

(a) Thermal and hydraulic transfer

Figure 7 shows the variation of the average Nusselt number of the fluid in the interior of the solar collector as a function of the Reynolds number for different values of turbulator height (turb_H) for a thickness turb_t = 2 mm, and at a certain volume concentration of CuO nanoparticles (φ = 3%). The Nusselt number increased approximately linearly with the Reynolds number with or without inserts. Thus, the average Nusselt number improved with increasing turbulator height. It can also be seen that, for the heights turb_H = 40 mm and 50 mm, they had almost the same profile of average Nusselt number evolution. The variation of the pressure difference (ΔP) as a function of Reynolds number with the turbulator of different heights is shown in Figure 8. However, as it can be seen, ΔP was larger when the height (turb_H) was large. Therefore, the pressure increased with increasing turbulator height. The maximum increase in ΔP was associated for the configuration with a height turb_H = 50 mm and a nanoparticle volume fraction φ = 3%. Figure 9 illustrates the effect of the Reynolds number on the coefficient of friction of the nanofluid for different values of turbulator height. In agreement with what is predicted in the literature, the results show a decrease in the friction loss coefficient with the increase of the Reynolds number. This reduction of the friction coefficient is based on its inversely proportional relationship with the Reynolds number. Thus, the friction coefficient increased with increasing height (turb_H). From these different results, we can deduce that the evolution of the thermal performance does not only cover the penalty of the increase of the pressure drop of the inserted turbulator, but it causes a gain in terms of heat transfer improvement.

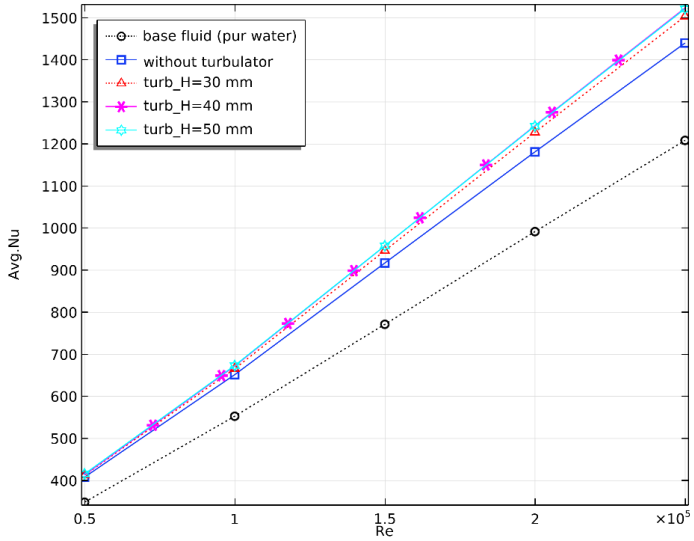

Figure 7. Evolution of the average Nusselt number of the fluid as a function of the Reynolds number for different heights (turb_H), with a thickness turb_t = 2 mm, for a nanoparticle concentration φ = 3%.

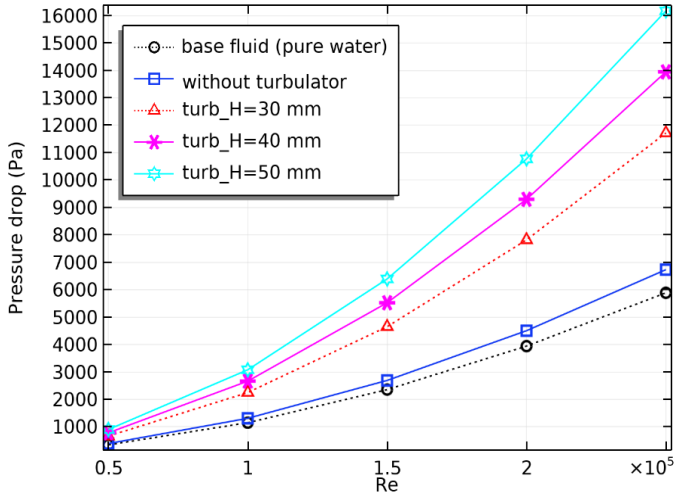

Figure 8. Profile of pressure drop of the fluid as a function of the Reynolds number for different heights (turb_H), with a thickness turb_t = 2 mm, for a nanoparticle concentration φ = 3%.

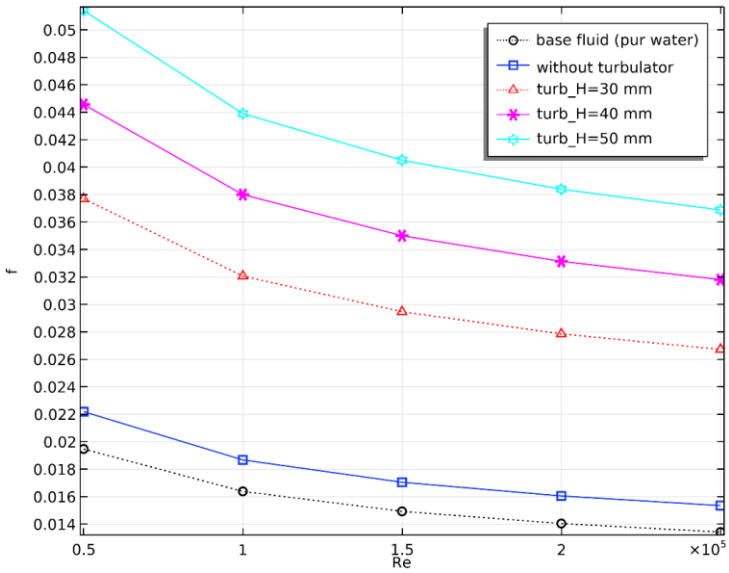

Figure 9. Variation of the friction coefficient as a function of the Reynolds number for different heights (turb_H), with a thickness turb_t = 2 mm, for a nanoparticle concentration φ = 3%.

(b) Thermal efficiency

It is interesting to study the thermal efficiency of the parabolic trough solar collector by inserting a turbulator into the absorber. Figure 10 shows the thermal efficiency for each height (turb_H) of the turbulator with the thickness (turb_t) set to 2 mm at different Reynolds numbers and a certain volume concentration of CuO nanoparticles (φ = 3%). It was revealed that the thermal efficiency started to increase for all different designs until it reached a Reynolds number Re = 100,000; then, it started to decrease for all different heights, with further increase in the Reynolds

number. As the Reynolds number increased, the pumping power also increased until the increase in pumping power became greater than the increase in useful energy delivered, resulting in a reduction in efficiency. Furthermore, it can be seen that the different turbulator heights had approximately the same thermal efficiency value for a Reynolds number Re = 250,000.

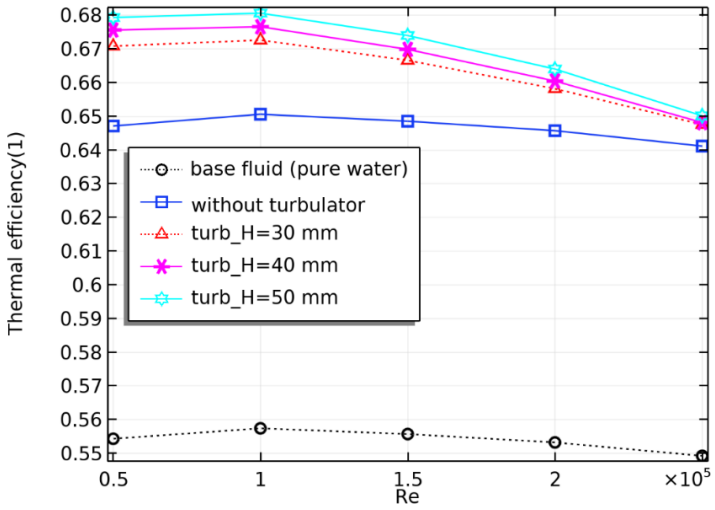

Figure 10. Variation of thermal efficiency as a function of the Reynolds number for different heights (turb_H), with a thickness turb_t = 2 mm, for a nanoparticle concentration φ = 3%.

(c) Temperature and velocity field distribution at the outlet

Due to the non-uniform distribution of the heat flux on the outer part of the absorber tube of the receiver, the temperature distribution of the receiver outlet should be non-uniform. Figure 11 shows the two-dimensional outlet temperature distribution for the CuO/water nanofluid (3%) with a turbulator thickness turb_t = 2 mm with different heights (turb_H) and a Reynolds number Re = 150,000. As the turbulator height (turb_H) increased, the thickness of the thermal boundary layer increased and the temperature distribution tended to become uniform. The progression of the outlet temperature for the turbulator with the increasing height (turb_H) can be noticed, as it generated a more marked turbulence, leading to a more important thermal boundary layer; and, the turbulator of height turb_H = 50 mm presented a great outlet temperature as compared to the other studied configurations. The profiles in Figure 12 show the evolution of the outlet velocity of the turbulator inserted in the absorber tube for different heights (turb_H) under the conditions of a thickness turb_t = 2 mm, Reynolds number Re = 150,000 and a nanofluid (CuO/water) with a certain volume concentration of nanoparticles (φ = 3%). It can be seen that the fluid in the tube had a maximum velocity at the center and tended toward zero at the wall. Indeed, the increase of the height of the turbulator (turb_H) led to a slowing down of the flow of the nanofluid inside the tube of the solar collector. The flow deceleration can be observed as the height (turb_H) value increased. We can also notice that the turbulator height (turb_H = 40 mm) resulted in a lower exit velocity than the other heights, which means that the turbulator was used to increase the thermal performance of the solar collector.

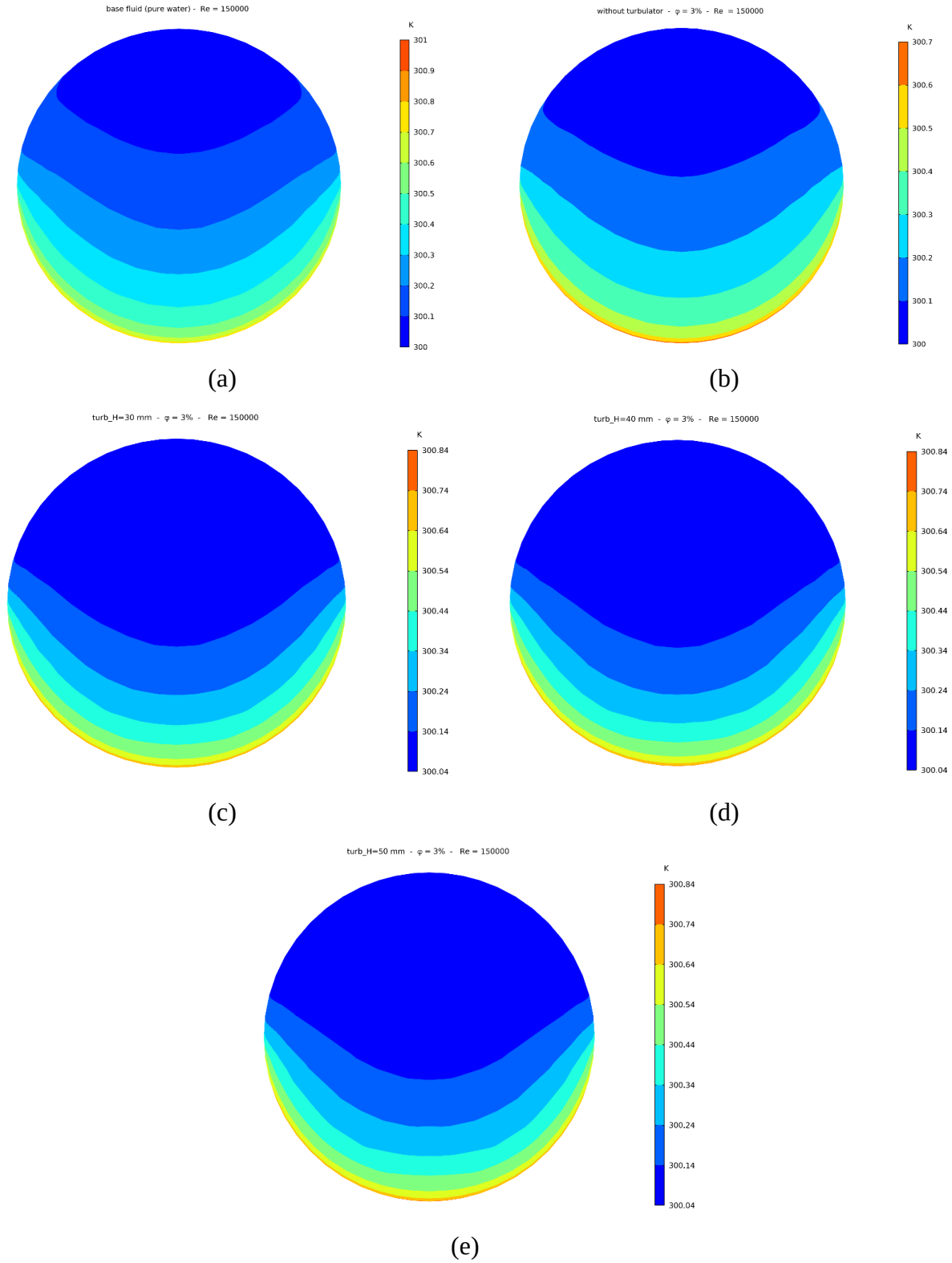

Figure 11. Profiles of absorber tube outlet temperature for different heights (turb_H), a thickness turb_t = 2 mm, Re = 150,000 and a nanoparticle concentration φ = 3%: (a) base fluid, (b) no turbulator, (c) turbulator height turb_H = 30 mm, (d) turbulator height turb_H = 40 mm, (e) turbulator height turb_H = 50 mm.

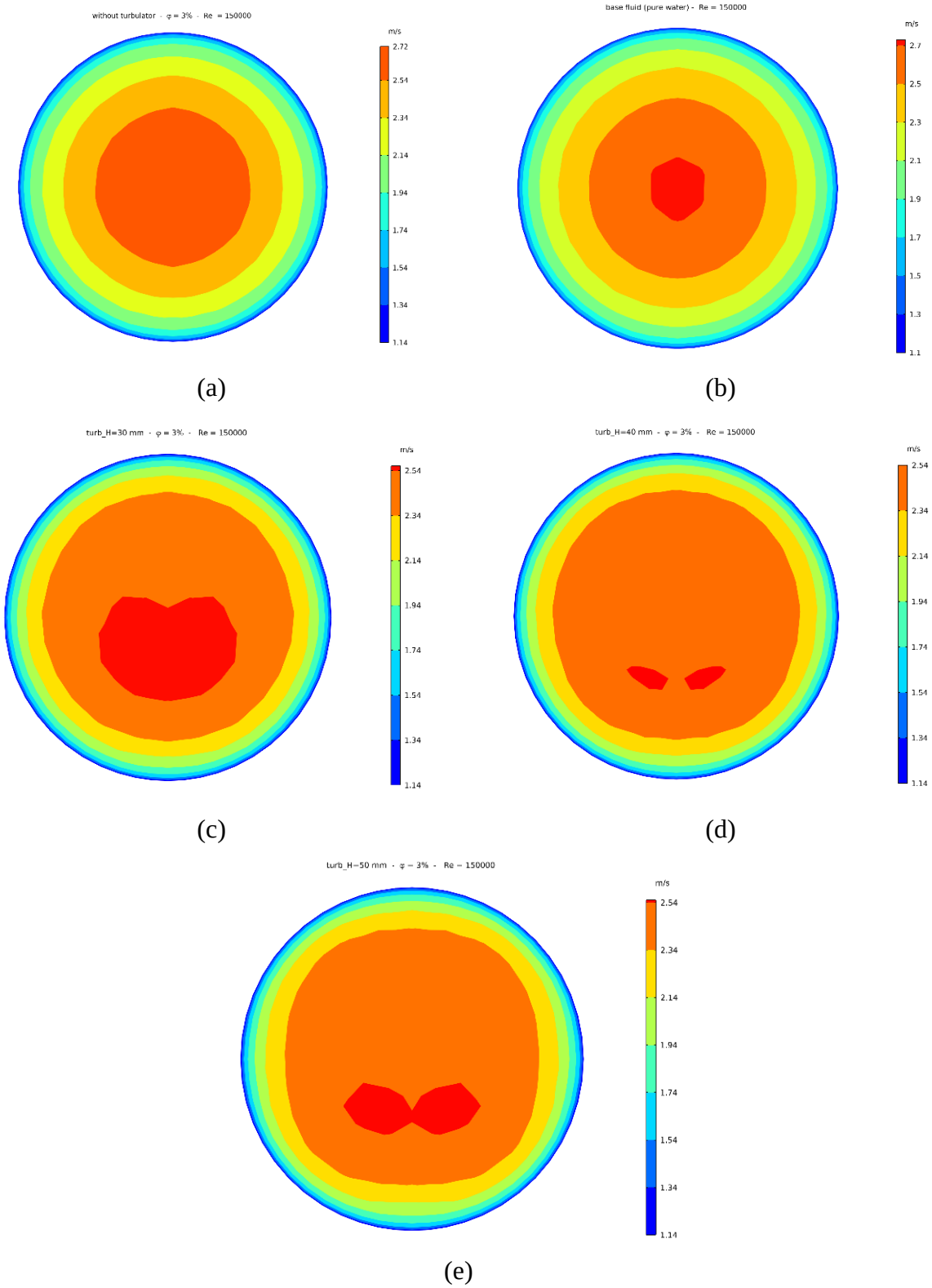

Figure 12. Profiles of absorber tube outlet velocity for different heights (turb_H), a thickness turb_t = 2 mm, Re = 150,000, a nanoparticle concentration φ = 3%: (a) base fluid, (b) no turbulator, (c) turbulator height turb_H = 30 mm, (d) turbulator height turb_H = 40 mm, (e) turbulator height turb_H = 50 mm.

4.1.2. Case 2: Turbulator height (turb_H = 40 mm) with different thicknesses (turb_t = 2, 4, 8 and 16 mm)

(a) Thermal and hydraulic transfer

Figure 13 shows the effect of the Reynolds number (Re) on the average Nusselt number for different thicknesses (turb_t), a height (turb_H) fixed at 40 mm and a (CuO/water) nanofluid concentration φ = 3%. It appears that the values of the average Nusselt number increased almost linearly with the increase of the Reynolds number, which induced an improvement of heat transfer in the solar collector. Significant improvements of the average Nusselt number can be observed for the case of thickness turb_t = 16 mm, followed by thicknesses turb_t = 8 mm, 4 mm and 2 mm. Figure 14 illustrates the variation of the pressure drop, which tended to increase with increasing Reynolds number, for pure water and the CuO/water nanofluid with the turbulator. It can be seen that, for all values of turbulator thickness, the pressure loss increased and the turbulator with a large thickness (turb_t = 16 mm) generated more pressure loss. Also, from the figure, it can be seen that pure water offered the lowest pressure drop. The variation of the friction coefficient as a function of the Reynolds number for different values of thickness (turb_t) for the height turb_H = 40 mm is shown in Figure 15. The latter illustrates that the friction coefficient decreased with increasing Reynolds number. Also, the turbulator with thickness turb_t = 16 mm had a large friction coefficient. Similarly, the friction coefficient decreased with the reduction of the turbulator thickness.

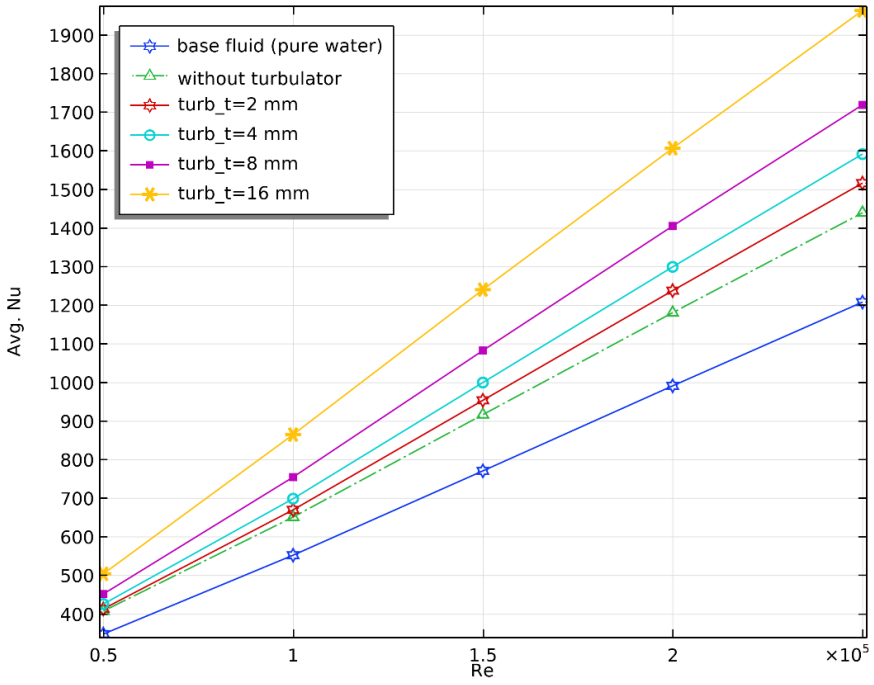

Figure 13. Evolution of the average Nusselt number as a function of the Reynolds number for different thicknesses (turb_t), a turbulator height turb_H = 40 mm and a nanoparticle concentration φ = 3%.

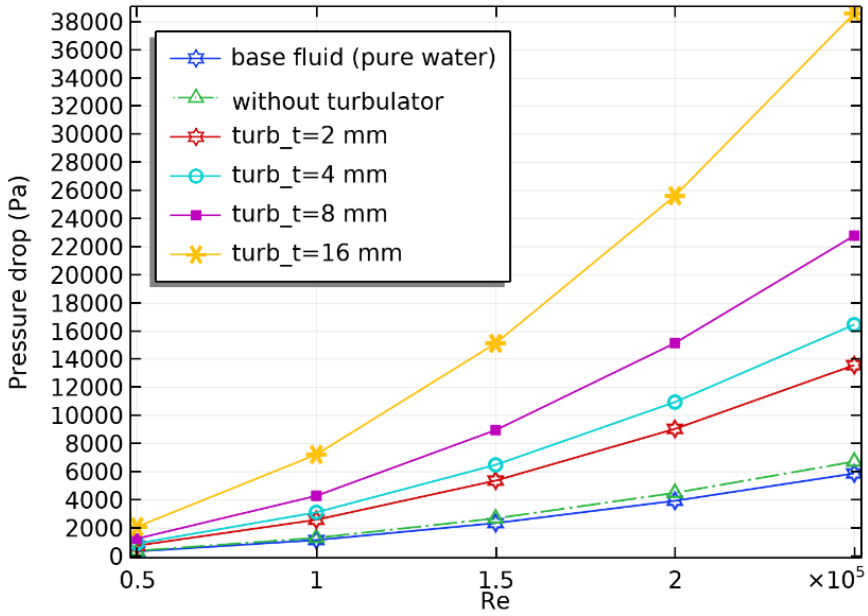

Figure 14. Profiles of pressure drop of the fluid as a function of the Reynolds number for different thicknesses (turb_t), a turbulator height turb_H = 40 mm and a nanoparticle concentration φ = 3%.

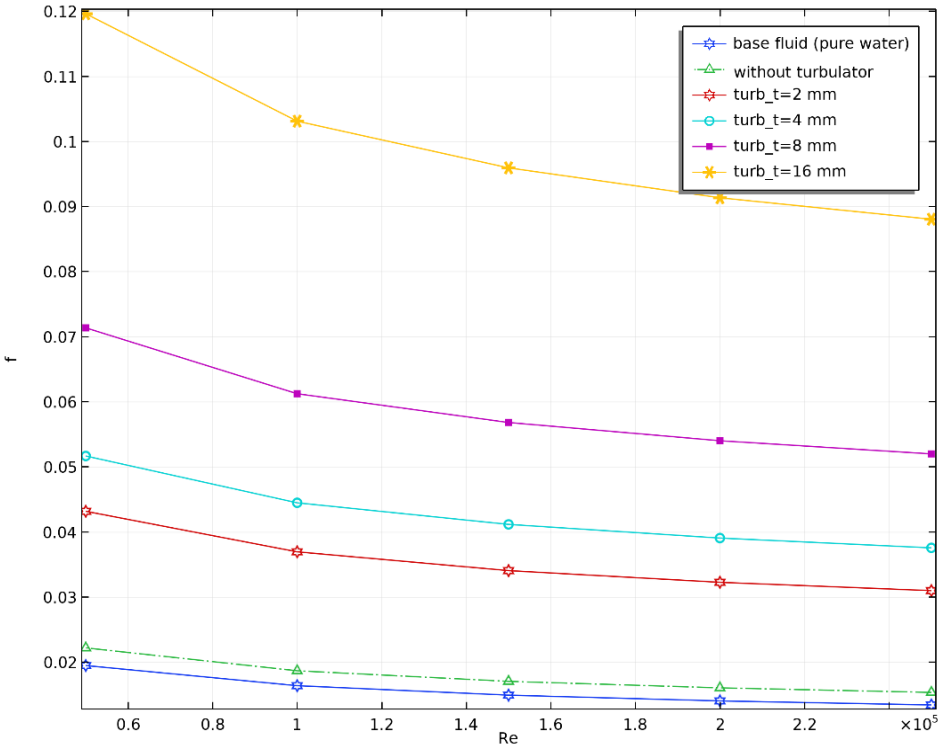

Figure 15. Evolution of the friction coefficient as a function of the Reynolds number for different thicknesses (turb_t), a turbulator height turb_H = 40 mm and a nanoparticle concentration φ = 3%.

(b) Thermal efficiency

The thermal efficiency is a key parameter in estimating the overall system performance. Figure 16 shows the evolution of the thermal efficiency of the solar collector as a function of the Reynolds number for the four turbulator thicknesses studied. It was found that the thermal efficiency increased for all different thicknesses, especially for low Reynolds numbers (until it reached Re = 100,000), and then started to decrease for all different thicknesses with further increase in the Reynolds number. The thermal efficiency was also better for the thickness (turb_t = 16 mm); for this case, it is remarkable that the Reynolds number Re = 50,000 was the best, because it can be seen that the efficiency decreased a little when the Reynolds number increased from 50,000 to 100,000, as shown in Figure 16. For higher Reynolds numbers, the pumping power increased significantly and reduced the efficiency to a lower level.

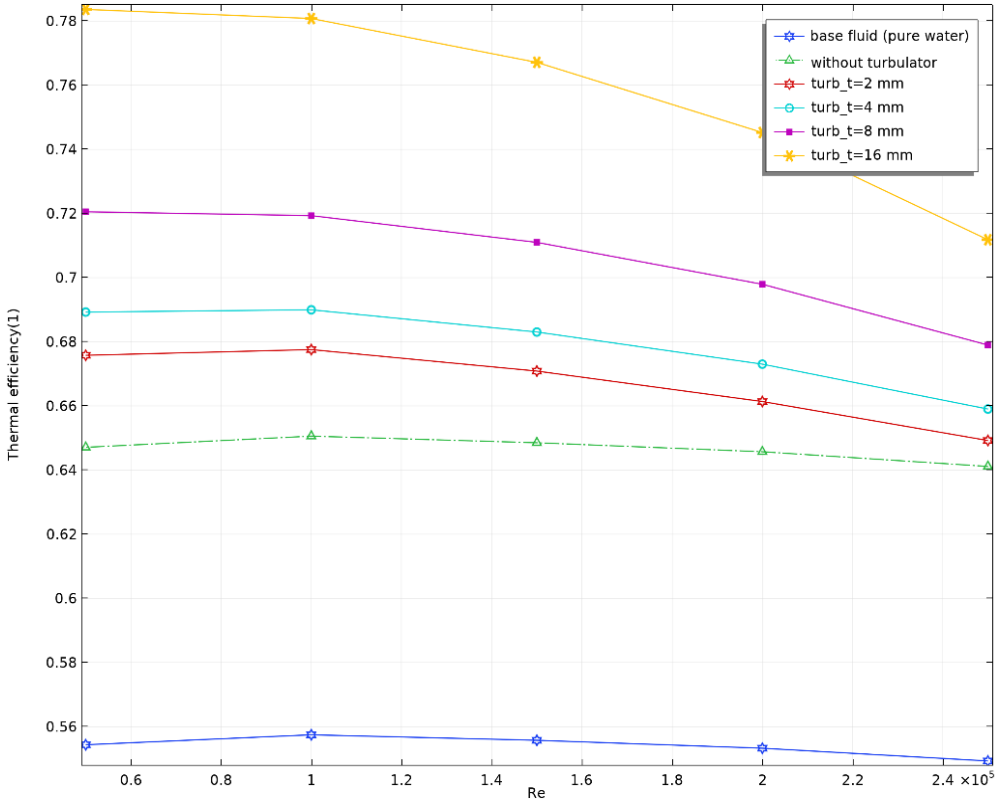

Figure 16. Profiles of thermal efficiency as a function of the Reynolds number for different thicknesses (turb_t), a turbulator height turb_H = 40 mm and a nanoparticle concentration φ = 3%.

(c) Temperature and velocity field distribution at the outlet

Due to the non-uniform distribution of the heat flow over the absorber tube of the receiver, the peripheral temperature distribution of the receiver should be non-uniform. The lower part of the absorber tube had a much higher heat flux than the upper part. Figure 17 shows the outlet temperature contours in the receiver for the base fluid (pure water), the CuO/water nanofluid with nanoparticle concentrations φ = 3% in the absorber without a turbulator and the nanofluid with a turbulator with a thickness turb_H = 40 mm and Reynolds number Re = 150,000. It can be seen in these figures that the outlet temperature increased with the insertion of the turbulator in the absorber. However, increasing the thickness of the turbulator improved the outlet temperature up to a thickness of 4 mm. Then, for the other thicknesses of 8 mm and 16 mm, the output temperature decreased. Furthermore, the turbulator with a thickness of 4 mm had the highest outlet temperature. Moreover, the turbulator with a thickness turb_t = 2 mm is suggested to be the configuration with similar performance to the configuration with a thickness turb_t = 4 mm with a reduced volume of the turbulator and, therefore, a reduced cost. Figure 18 illustrates the contours of the absorber tube outlet velocity for different thicknesses (turb_t) and for a Reynolds number Re = 150,000 for the nanofluid (CuO/water) with a nanoparticle volume concentration φ = 3%. Thus, an increase in the turbulator thickness (turb_t) led to a slowing down of the nanofluid velocity and a widening of the velocity field inside the solar collector tube. It is also observed that increasing the thickness of the inserted turbulator contributed to a change in the velocity distribution, whereas the thickness increased and the modifies the morphology of the flow. This phenomenon is thought to be due to the presence of a vortex flow that contributed to heat exchange. We also note that both thicknesses tub_t = 8 and 16 mm resulted in the same exit velocity.

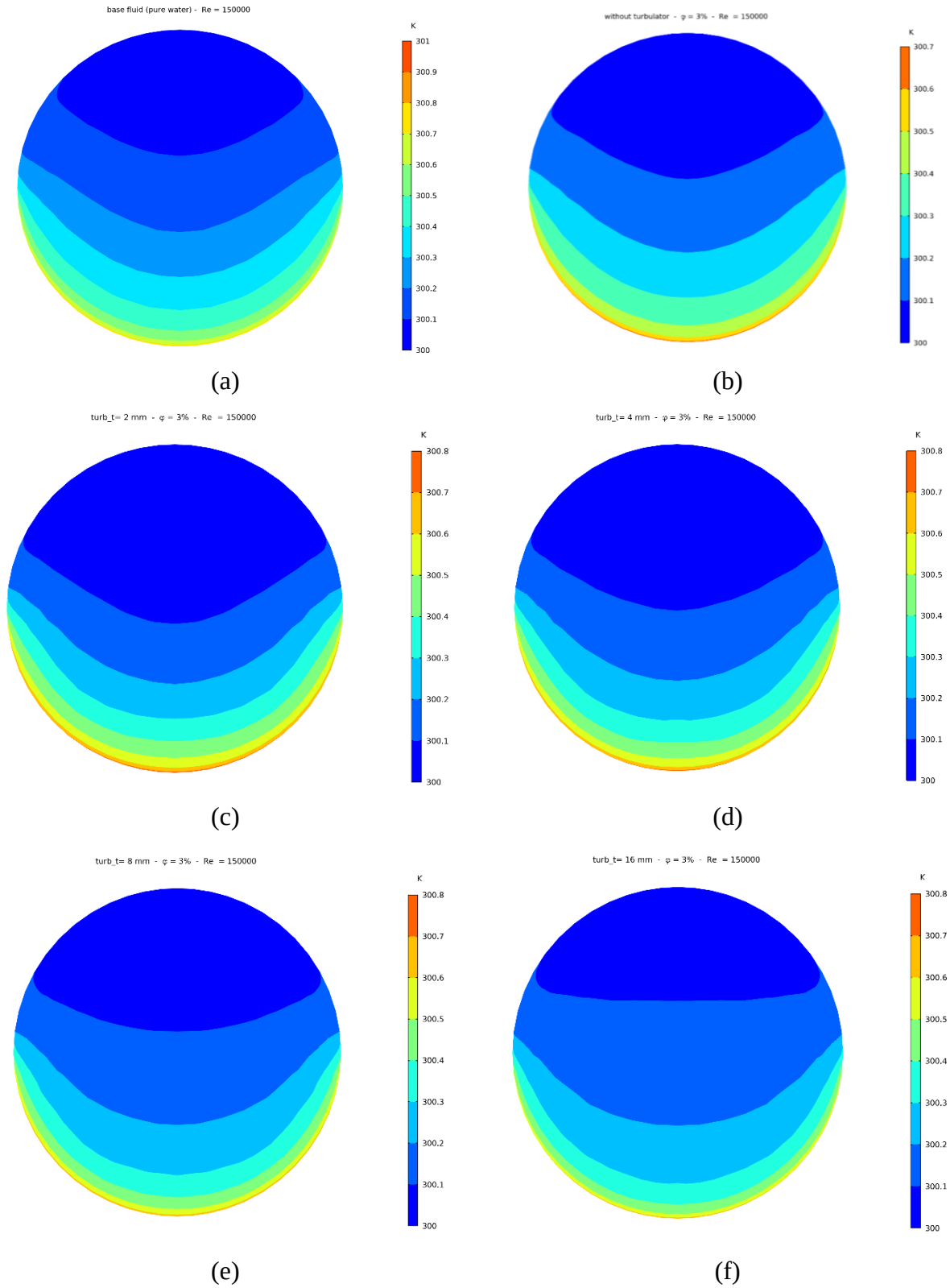

Figure 17. Profiles of absorber tube outlet temperature for different thicknesses (turb_t), a turbulator height turb_H = 40 mm, Re = 150,000 and a nanoparticle concentration φ = 3%: (a) base fluid, (b) without turbulator, (c) turbulator thickness turb_t = 2 mm, (d) turbulator thickness turb_t = 4 mm, (e) turbulator thickness turb_t = 8 mm, (f) turbulator thickness turb_t = 16 mm.

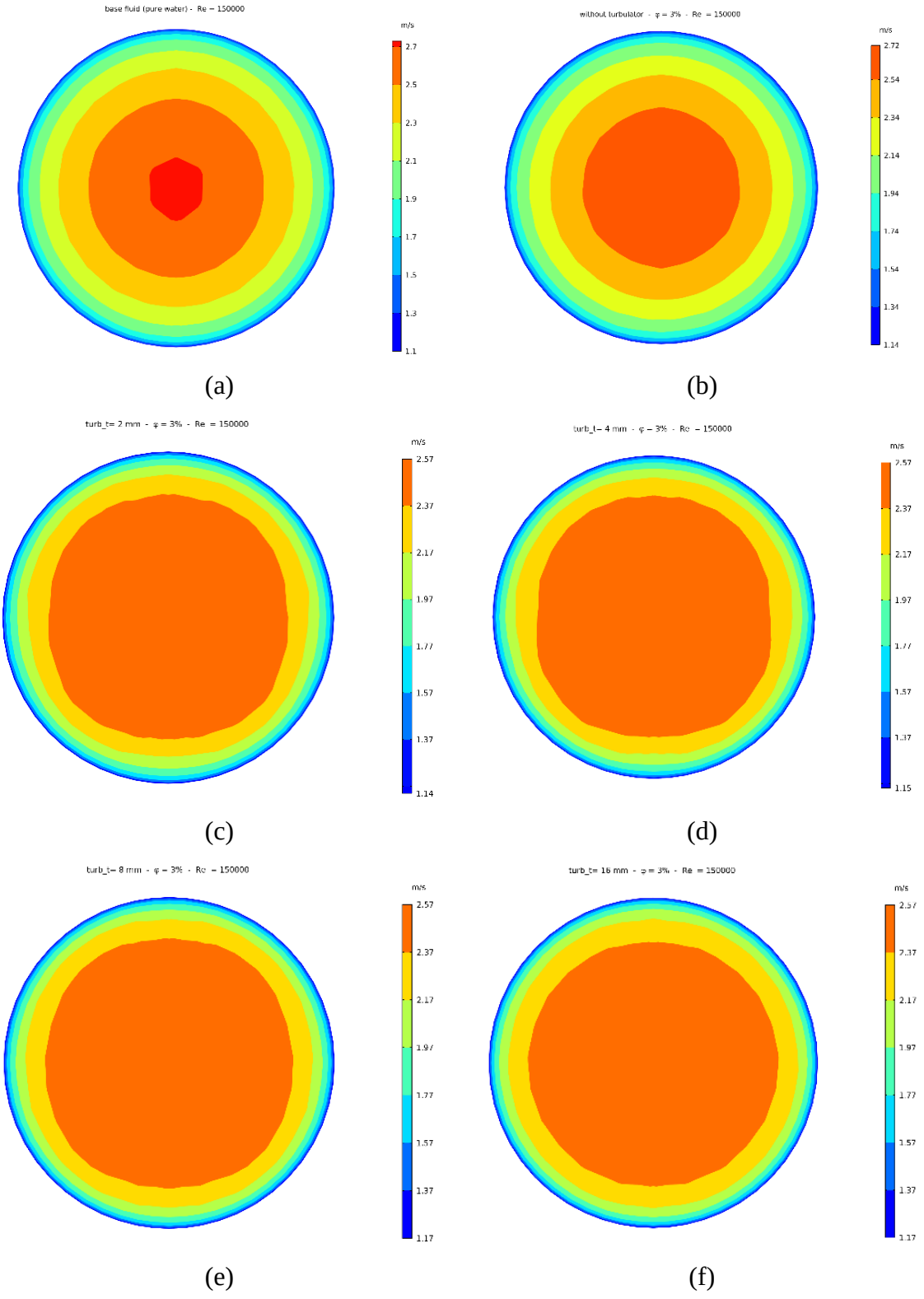

Figure 18. Velocity profiles of the absorber tube outlet velocity for different thicknesses (turb_t), a turbulator height turb_H = 40 mm, Re = 150000 and a nanoparticle concentration φ = 3%: (a) base fluid, (b) without turbulator, (c) turbulator thickness turb_t = 2 mm, (d) turbulator thickness turb_t = 4 mm, (e) turbulator thickness turb_t = 8 mm, (f) turbulator thickness turb_t = 16 mm.

4.2. Effect of twisted turbulator geometry (N_twist = 5, 10 and 15 twists)

4.2.1. Thermal and hydraulic transfer

Figure 19 presents the variation of the average Nusselt number as a function of the Reynolds number for the absorber, with all geometrical configurations shown in the figure for the CuO/water nanofluid with a nanoparticle volume concentration φ = 3%. It can be seen that the Nusselt number increased with the Reynolds number, which improved the heat transfer coefficient in the absorber. A significant improvement in the average Nusselt number can be observed for the twisted turbulator (N_twist = 15 twists). It can be seen that the turbulator with a thickness turb_t = 2 mm, height turb_H = 40 mm and N_twist = 5 twists had the same average Nusselt number. In general, the increase in heat transfer by the twisted turbulator technique generated pressure losses. The effects of the twisted tubulator on the pressure drop values are shown in Figure 20. This illustration shows the variation of the pressure drop with increasing Reynolds number. It can be seen that ΔP increased with increasing Reynolds number. The twisted turbulators produced a higher pressure drop value than the absorber without a turbulator. The turbulator with the dimensions turb_t = 2 mm and turb_H = 40 mm had a higher pressure drop value than the turbulator with five twists. The twisted turbulator with 15 twists generated a higher pressure drop value than the other configurations. Figure 21 shows the variation of the friction coefficient (f) as a function of the Reynolds number. The friction coefficient decreased with increasing Reynolds number in the turbulent flow regime, as shown in the figure. It is remarkable that the twisted turbulator with 15 twists had a large friction coefficient. The absorber with the nanofluid (CuO/water) without a turbulator and the absorber with the base fluid (pure water) each had good friction coefficients.

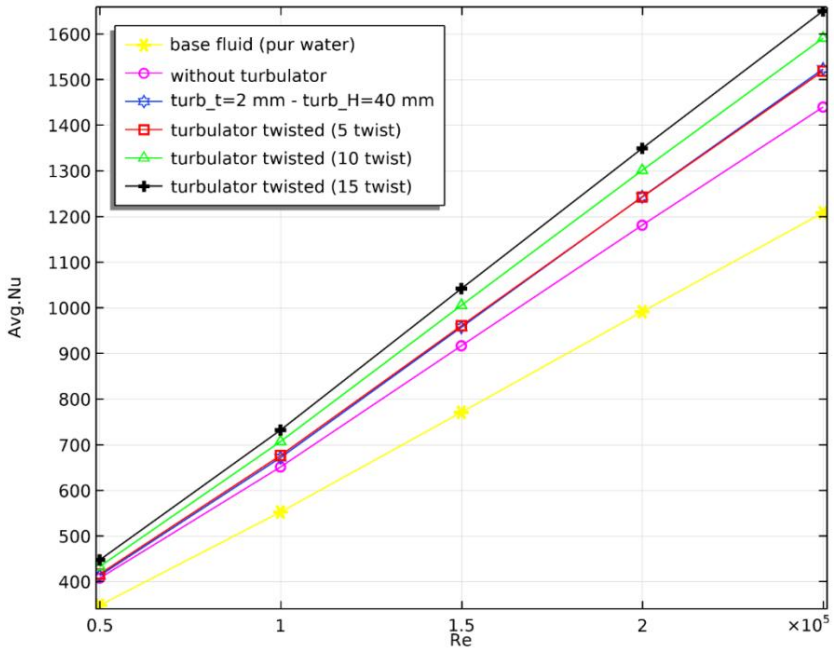

Figure 19. Evolution of the average Nusselt number as a function of the Reynolds number for different twisted turbulators (N_twist = 5, 10 and 15 twists) and a nanoparticle concentration φ = 3%.

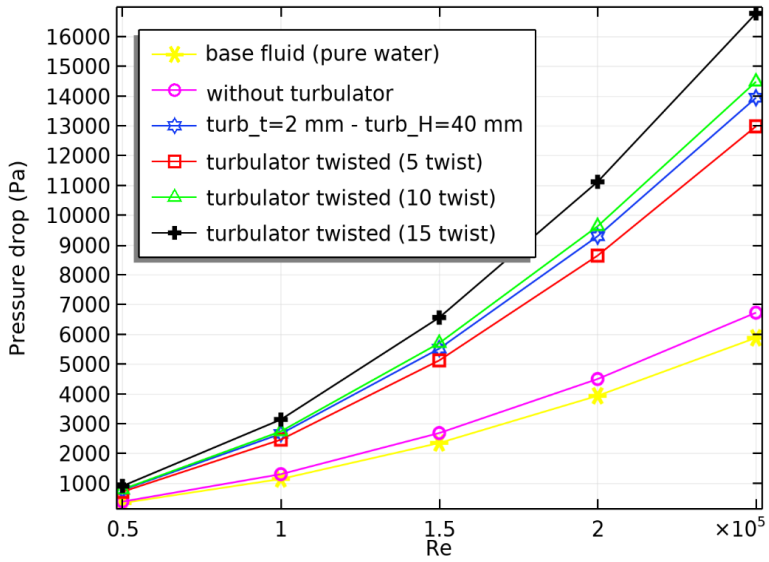

Figure 20. Profiles of pressure drop as a function of the Reynolds number for different twisted turbulators (N_twist = 5, 10 and 15 twists) and a nanoparticle concentration φ = 3%.

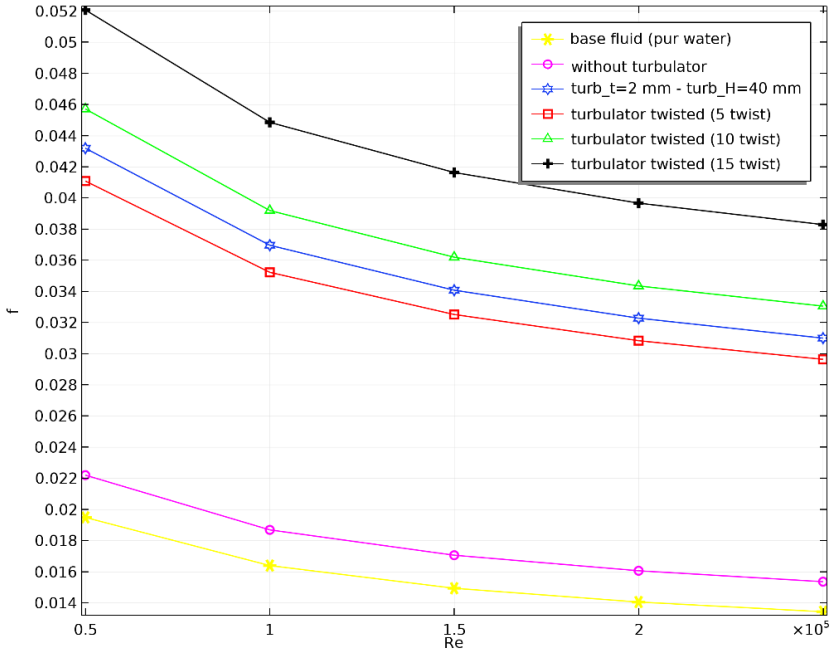

Figure 21. Coefficient of friction profiles as a function of the Reynolds number and different twisted turbulators (N_twist = 5, 10 and 15 twists) and a nanoparticle concentration φ = 3%.

4.2.2. Thermal efficiency

Figure 22 shows the evolution of the thermal efficiency of the solar collector with different twisted turbulator configurations (N_twist = 5, 10 and 15 twists), where the turbulator was inserted

inside the absorber and the CuO/water nanofluid had a nanoparticle volume concentration of 3%. As shown in this figure, the highest efficiency was associated with the Reynolds number Re = 100000. Furthermore, for higher Reynolds numbers, the efficiency decreased due to an increase in the pressure drop value. The figure shows that the turbulator with a height of 40 mm and thickness of 2 mm had better thermal performance than the twisted turbulator (with 5, 10 and 15 twists). Also, the 5-twist turbulator had good efficiency compared to the 10- and 15-twist turbulators.

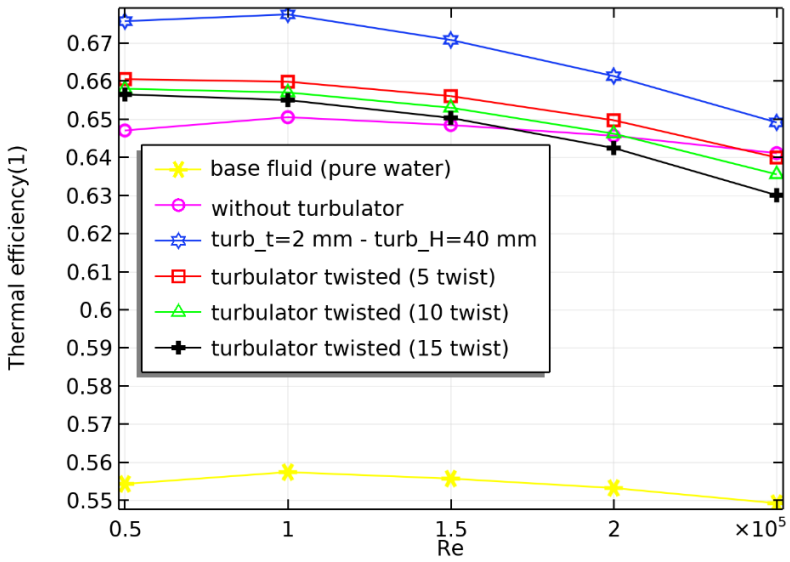

Figure 22. Thermal efficiency as a function of the Reynolds number for different twisted turblators (N_twist = 5, 10 and 15 twists) and a nanoparticle concentration φ = 3%.

4.2.3. Temperature and velocity field distribution at the outlet

Figure 23 shows the two-dimensional distribution of the receiver tube outlet temperature for the CuO/water nanofluid at a nanoparticle volume concentration φ = 3%, a twisted turbulator with 5, 10 or 15 twists, and a Reynolds number Re = 150000. Due to the non-uniform heat flow on the outer wall of the absorber, we noticed that the lower part of the collector showed interesting temperature variations for all configurations. We can see that the turbulator with the dimensions turb_t = 2 mm and turb_H = 40 mm had an interesting temperature as compared to the other configurations. As shown in Figure 23d–f, the use of a twisted turbulator gave a more uniform temperature distribution around the circumference of the receiver tube as compared to a regular receiver tube. The turbulator with five twists had an interesting output temperature as compared to the 10- and 15-twist turbulator. Figure 24 presents the output velocity field distributions for the twisted turbulators with 5, 10 or 15 twists inserted into the absorber tube, where the Reynolds number Re = 150000 for the nanofluid (CuO/water) with a nanoparticle volume concentration φ = 3%. However, the increase in twist number for the twisted turbulator led to a moderate delay in the flow of the nanofluid and a larger velocity field inside the solar collector tube. It can also be seen that an increase in the number of twists contributed to a decrease in the velocity distribution toward the lower part of the solar collector, as shown in Figure 24, which led to a slowing down that improved the heat exchange.

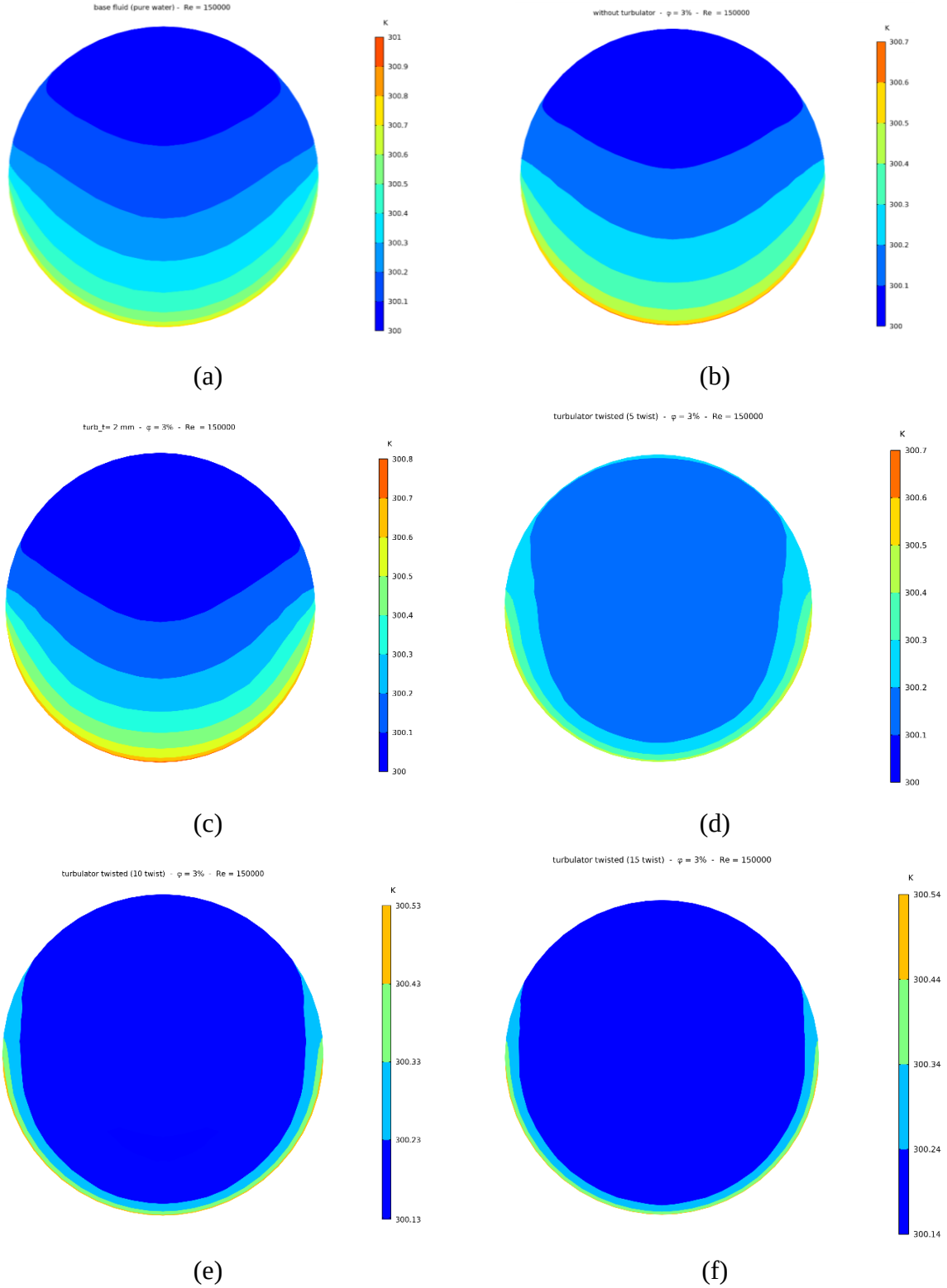

Figure 23. Absorber tube outlet temperature distribution for the twisted turbulator with turb_t = 2 mm and turb_H = 40 mm, given Re = 150000 and a nanoparticle concentration φ = 3%: (a) base fluid, (b) no turbulator, (c) turb_t = 2 mm and turb_H = 40 mm, (d) twisted turbulator (five twists), (e) twisted turbulator (10 twists), (f) twisted turbulator (15 twists)

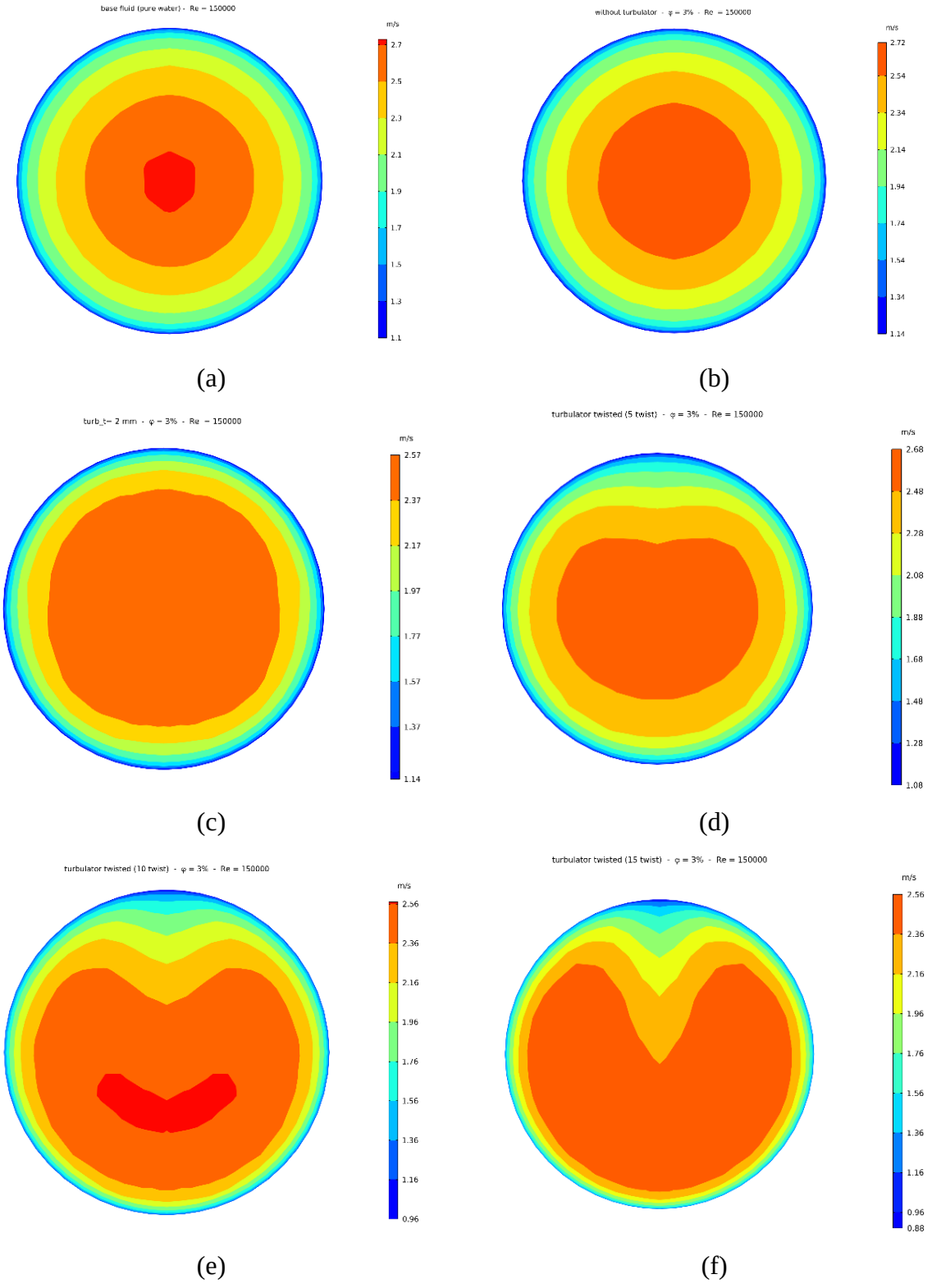

Figure 24. Absorber tube outlet velocity field distribution for the twisted turbulator of turb_t = 2 mm and turb_H = 40 mm, given Re = 150000 and a nanoparticle concentration φ = 3%: (a) base fluid, (b) no turbulator, (c) turb_t = 2 mm and turb_H = 40 mm, (d) twisted turbulator (five twists), (e) twisted turbulator (10 twists), (f) twisted turbulator (15 twists).

5. Conclusion

This paper investigates the effects of inserting a turbulator with dimensions of turb_t = 2 mm and turb = 40 mm, with no twisted configuration. First, the effects of different heights (turb_H = 30 mm, 40 mm, 50 mm) and different thicknesses (turb_t = 2 mm, 4 mm, 8 mm, 16 mm) were examined. A twisted turbulator with five, 10 and 15 twists was studied next. The three-dimensional numerical study was performed for the Reynolds number ranging from 50000 to 250000 and a CuO/water nanofluid volume fraction of 3%. The graphs of heat transfer, pressure drop, friction factor, thermal efficiency and temperature and exit velocity contours have been presented and analyzed. The results were as follows:

(1) Increasing the Reynolds number had the effects of increasing the heat transfer, the flow field and the pressure drop.
(2) Increasing the turbulator height led to an increase in the Nusselt number as well as pressure difference and friction factor.
(3) The outlet temperature increased in the lower part of the absorber as the turbulator height increased, but the output velocity decreased.
(4) The evolution of the Reynolds number indicated that the average Nusselt number and the friction factor tends to increase with the increase of the turbulator thickness.
(5) The temperature and the outlet velocity decreased with the increase of the turbulator thickness.
(6) The increase in the number of twists of the turbulator led to an increase in the average Nusselt number.
(7) The temperature and outlet velocity decreased with increasing number of twists.
(8) The twisted turbulator resulted in worse performance than the simple turbulator.

Conflict of Interest

The authors declare no conflict of interest.

References

1. Shahbaz M, Raghutla C, Chittedi KR, et al. (2020) The effect of renewable energy consumption on economic growth: Evidence from the renewable energy country attractive index. *Energy* 207: 118162. https://doi.org/10.1016/j.energy.2020.118162
2. Bellos E, Tzivanidis C (2019) Alternative designs of parabolic trough solar collectors. *Prog Energy Combust Sci* 71: 81–117. https://doi.org/10.1016/j.pecs.2018.11.001
3. Ouabouch O, Laasri IA, Kriraa M, et al. (2022) Effects of flow regime and geometric parameters on the performance of a parabolic trough solar collector using nanofluid. *Numer Heat Transf Part A App* 82: 1–13. https://doi.org/10.1080/10407782.2022.2078632
4. Tembhare SP, Barai DP, Bhanvase BA(2022) Performance evaluation of nanofluids in solar thermal and solar photovoltaic systems: A comprehensive review. *Renew Sustain Energy Rev* 153: 111738. https://doi.org/10.1016/j.rser.2021.111738

5. Qi C, Luo T, Liu M, et al. (2019) Experimental study on the flow and heat transfer characteristics of nanofluids in double-tube heat exchangers based on thermal efficiency assessment. *Energy Convers Manag* 197: 111877. https://doi.org/10.1016/j.enconman.2019.111877
6. Choi SUS, Eastman JA (1995) Enhancing thermal conductivity of fluids with nanoparticles. *1995 International mechanical engineering congress and exhibition, San Francisco, CA (United States*.
7. Ouabouch O, Kriraa M, Lamsaadi M (2021) Stability, thermophsical properties of nanofluids, and applications in solar collectors: A review. 8: 659–684. https://doi.org/10.3934/matersci.2021040
8. Ghasemi SE, Ranjbar AA (2016) Thermal performance analysis of solar parabolic trough collector using nanofluid as working fluid: A CFD modelling study. *J Mol Liq* 222: 159–166. https://doi.org/10.1016/j.molliq.2016.06.091
9. Ouabouch O, Laasri IA, Kriraa M, et al. (2021) Modelling and comparison of the thermohydraulic performance with an economical evaluation for a parabolic trough solar collector using different nanofluids. *Int J Heat Technol* 39: 1763–1769. https://doi.org/10.18280/ijht.390609
10. Bellos E, Tzivanidis C, Antonopoulos KA, et al. (2016) Thermal enhancement of solar parabolic trough collectors by using nanofluids and converging-diverging absorber tube. *Renew Energy* 94: 213–222. https://doi.org/10.1016/j.renene.2016.03.062
11. Garc á A, Vicente PG, Viedma A (2005) Experimental study of heat transfer enhancement with wire coil inserts in laminar-transition-turbulent regimes at different Prandtl numbers. *Int J Heat Mass Transf* 48: 4640–4651. https://doi.org/10.1016/j.ijheatmasstransfer.2005.04.024
12. Mwesigye A, Bello-Ochende T, Meyer JP (2015) Multi-objective and thermodynamic optimisation of a parabolic trough receiver with perforated plate inserts. *Appl Therm Eng* 77: 42–56. https://doi.org/10.1016/j.applthermaleng.2014.12.018
13. Khan MS, Yan M, Ali HM, et al. (2020) Comparative performance assessment of different absorber tube geometries for parabolic trough solar collector using nanofluid. *J Therm Anal Calorim* 142: 2227–2241. https://doi.org/10.1007/s10973-020-09590-2
14. Liu Y, Chen Q, Hu K, et al. (2016) Flow field optimization for the solar parabolic trough receivers in direct steam generation systems by the variational principle. *Int J Heat Mass Transf* 102: 1073–1081. https://doi.org/10.1016/j.ijheatmasstransfer.2016.06.083
15. Saedodin S, Zaboli M, Ajarostaghi SSM (2021) Hydrothermal analysis of heat transfer and thermal performance characteristics in a parabolic trough solar collector with Turbulence-Inducing elements. *Sustain Energy Techn* 46: 101266. https://doi.org/10.1016/j.seta.2021.101266
16. Olfian H, Ajarostaghi SSM, Farhadi M, et al. (2021) Melting and solidification processes of phase change material in evacuated tube solar collector with U-shaped spirally corrugated tube. *Appl Therm Eng* 182: 116149. https://doi.org/10.1016/j.applthermaleng.2020.116149
17. Fan F, Qi C, Liu Q, et al. (2020) Effect of twisted turbulator perforated ratio on thermal and hydraulic performance of magnetic nanofluids in a novel thermal exchanger system. *Case Stud. Therm Eng* 22: 100761. https://doi.org/10.1016/j.csite.2020.100761

18. Song X, Dong G, Gao F, et al. (2014) A numerical study of parabolic trough receiver with nonuniform heat flux and helical screw-tape inserts. *Energy* 77: 771–782. https://doi.org/10.1016/j.energy.2014.09.049
19. Khanafer K, Vafai K (2011) A critical synthesis of thermophysical characteristics of nanofluids. *Int J Heat Mass Transf* 54: 4410–4428. https://doi.org/10.1016/j.ijheatmasstransfer.2011.04.048
20. Xuan Y, Roetzel W (2000) Conceptions for heat transfer correlation of nanofluids. *Int J Heat Mass Transf* 43: 3701–3707. https://doi.org/10.1016/S0017-9310(99)00369-5
21. Brinkman HC (1952) The viscosity of concentrated suspensions and solutions. *J Chem Phys* 20: 571. https://doi.org/10.1063/1.1700493
22. Maxwell JC (1891) *A Treatise on Electricity and Magnetism*, UK: Clarendon Press.
23. Turkyilmazoglu M (2017) Condensation of laminar film over curved vertical walls using single and two-phase nanofluid models. *Eur J Mech B/Fluids* 65: 184–191. https://doi.org/10.1016/j.euromechflu.2017.04.007
24. Yuan SW (1967) *Foundations of Fluid Mechanics*, New York: Prentice-Hall.
25. Chakraborty O, Das B, Gupta R, et al. (2020) Heat transfer enhancement analysis of parabolic trough collector with straight and helical absorber tube. *Therm Sci Eng Prog* 20: 100718. https://doi.org/10.1016/j.tsep.2020.100718
26. Petukhov BS (2017) Heat transfer and friction in turbulent pipe flow with variable physical properties. *Adv Heat Transf* 6: 503–564. https://doi.org/10.1016/S0065-2717(08)70153-9

AIMS Press